

Soft and Hard Adhesion

Jun Young Chung
Manoj K. Chaudhury

Department of Chemical Engineering, Lehigh University, Bethlehem,
Pennsylvania, USA

The force needed to pull a cylindrical stud from a soft elastomeric film depends on their elastic and geometric properties. For a rigid stud and a thick elastomeric film, the pull-off stress (σ) depends on the elastic modulus (E) of the film and the radius (a) of the stud as $\sigma \sim (E/a)^{1/2}$ (soft adhesion). However, when the film is very thin, the pull-off stress is significantly higher than the case with thick films, and its value depends on the elastic modulus and the thickness (h) of the film as $\sigma \sim (E/h)^{1/2}$ (hard adhesion). Here, we study the pull-off behavior of a soft cylindrical stud, one flat end of which is coated with a high modulus thin baseplate. As the flexural rigidity of this baseplate is varied, we observe the transition between the two types of adhesion. We present a simple physical interpretation of the problem, which could be of value in understanding various biofouling and adhesive situations.

Keywords: Adhesion; Adhesion of plates; Biofouling; Elastomer adhesion; Mechanics of adhesion; Pull-off test; Silicone release coatings

I. INTRODUCTION

Kendall [1] employed the energy balance criterion of Griffith [2] to study the adhesion and fracture at soft interfaces under various settings. Among his numerous contributions, a special case involves pulling rigid studs from soft elastic layers. In recent years, considerable attention has been paid to these classes of problems in the context of

Received 21 June 2005; in final form 8 August 2005.

One of a collection of papers honoring Manoj K. Chaudhury, the February 2005 recipient of The Adhesion Society Award for Excellence in Adhesion Science, sponsored by 3M.

Address correspondence to Manoj K. Chaudhury, Department of Chemical Engineering, Iacocca Hall, 111 Research Drive, Lehigh University, Bethlehem, PA 18015, USA. E-mail: mkc4@lehigh.edu

understanding, among others, the adhesion of rigid objects to soft materials [3–10] and the release behavior of fouling organisms [11–13] from various surfaces.

Next to Kendall's pioneering contributions, the most comprehensive studies to date in this field are those of Shull, Creton, and their collaborators [5–10], who used the probe tack test to examine varieties of situations: fully confined films (thickness of the film being much smaller than the stud radius), unconfined films, and films of intermediate confinements. Although the extreme situations of confined and unconfined films as studied by these authors are in general agreement with those of Kendall [1], Shull *et al.* [5, 8, 10] also proposed a valuable interpolating equation, supported by finite element analysis, that can be used for films of intermediate confinements. By measuring the stress in the film as a function of displacement, these authors successfully verified the predictions of their theoretical analysis [7, 8, 10].

Singer *et al.* [11, 12] and Chaudhury *et al.* [13] applied Kendall's methodologies to study fouling release problems. Fouling organisms readily colonize marine vessels. One of the strategies that is being investigated in the ONR (office of Naval Research) program in the United States is to promote easy removal of the foulants from naval vessels by painting them with organic coatings. Most fouling organisms secrete adhesive films, which interact either strongly or weakly with organic coatings. However, even when weak interaction prevails, it is not an easy task to remove the organisms from surfaces, because they maximize adhesion by manipulating the mechanical and geometric properties of the adhesives. Some organisms [13–15] could maximize the removal stress with adhesives that spread on a surface by thinning progressively so that the stress singularity at the edge of contact is weakened. Barnacles [16–18], conversely, use relatively thick and high modulus adhesive, removal of which is difficult because it is incapable of storing sufficient elastic energy by deformation under moderate external stress. Marine mussels [19] maximize adhesion by distributing the force to multiple attachment sites that act independently. However, the encouraging finding is that the polymeric films of low modulus and low surface energy do promote easy release of foulants [11–13, 16–18]. The mechanisms underlying the release of foulants from the soft films can be understood, at least qualitatively, in the light of the pioneering studies by Kendall [1] and Shull *et al.* [5–10]. Quantitative prediction of the release force, however, is rather difficult because of the complex interplay of the various properties of the organisms and coatings.

Here, we examine the adhesion and fracture of a model foulant with an elastomeric film using an axisymmetric pull-off test along the same

line as those pioneered by Creton and Lakrout [7] and Shull *et al.* [5–10], but with a difference in the model system. The model foulant, in our studies, is created by bonding a thin baseplate to one flat end of a soft elastomeric stud. The rigidity and the dimension of the baseplate are varied over a wide range to delineate the transition between hard- and soft-fouling releases. We attempt to present a simple physical interpretation of the problem with the hope that it would be of value in dealing with biofouling and other adhesive situations.

II. RESULTS AND DISCUSSION

Description of the Model

We begin with a brief introductory review of the main result of linear elastic fracture mechanics (LEFM) that is used for subsequent discussions. More detailed presentation of this kind of analysis can be found in Reference [10]. LEFM assumes that all elastic deformations follow Hooke's law, in which the elastic strain energy ($U_E = \int Fd\delta$) for a system is expressed in terms of either a force-stiffness or a displacement-stiffness relationship:

$$U_E = \frac{1}{2} \frac{F^2}{k} \text{ or } U_E = \frac{1}{2} \delta^2 k, \quad (1)$$

where F is the tensile force, k is the stiffness or spring constant of the system, and δ is the tensile displacement. The ratio of force to displacement k is defined as: $k = F/\delta$. Applying Griffith's fracture criterion [2] to Equation (1), one obtains the strain energy release rate (G_c) as

$$G_c = - \left. \frac{\partial U_E}{\partial A} \right|_{F_c} = - \frac{F_c^2}{2} \frac{\partial(1/k)}{\partial A}, \quad (2)$$

where A is the circular area of contact ($A = \pi a^2$) and F_c is the critical pull-off force. For nondissipative systems, G_c is equivalent to the thermodynamic work of adhesion (W). Rearranging Equation (2) yields the critical pull-off stress, $\sigma_c = F_c/\pi a^2$, as

$$\sigma_c = \sqrt{-4W / \left\{ \pi a^3 \left[\frac{\partial(1/k)}{\partial a} \right] \right\}}. \quad (3)$$

We now turn our attention to a model system, which consists of an elastomeric rubber block bonded to a flexible baseplate (Figure 1). The elastic block is the surrogate for a soft tissue with finite modulus, whereas

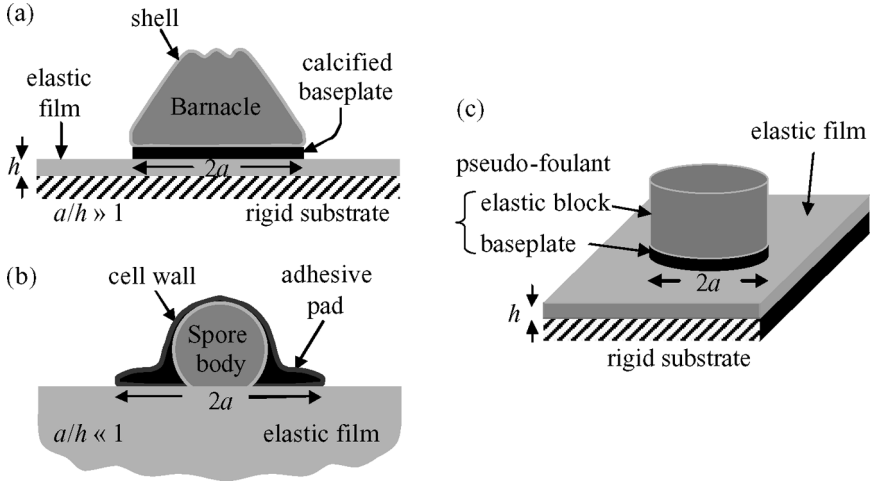


FIGURE 1 Schematics of the fouling species adhering to an elastic film: (a) adhesion of barnacle larva (macroscopic hard foulant) and (b) adhesion of spore of algae (microscopic soft foulant). (c) The model system.

the baseplate represents the properties of thin bioadhesive layer with finite flexural rigidity. The baseplate of this composite model system is brought into contact with a thin elastomeric film bonded to a rigid substrate. Our objective is to find the relationship between the force needed to pull this structure from the thin elastomeric film as a function of the elastic and geometric properties of all the components involved. Although this model system does not capture all the details of real foulants (for example, the effects of the side walls are ignored), it is, nonetheless, a useful simplification of the complex fouling organisms. Studying this model system could be of value in terms of posing relevant questions for real fouling-release situations.

When the model adhesive is subjected to a tensile force, the whole elastic body deforms (Figure 2). In principle, the overall deformation behavior can be described in terms of the coupled differential equations of deformation of the individual structural members and by a set of corresponding boundary conditions. Instead of attempting a complete elastic solution of this kind, we employ a simple approach in which individual elastic bodies of the system are represented by mechanical springs and determine the contribution of each component (elastic film, flexible baseplate and elastic block) separately. Once the behaviors of the components are understood, we attempt to describe the behavior of the composite system in a semi-empirical fashion.

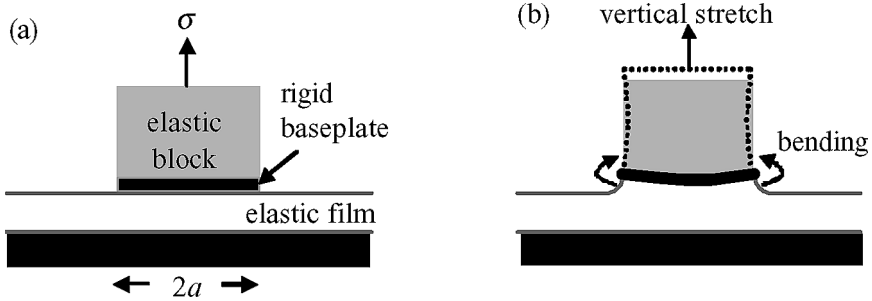


FIGURE 2 Further details of the model system: (a) the contact between a pseudo-foulant and an elastic film and (b) sketch showing that a vertical stretch in the cylindrical block leads to bending in the baseplate.

Pull-out of a Rigid Cylinder from a Soft Elastic Film

We consider a system, where a smooth-ended rigid cylindrical stud of radius a is initially in contact with a soft elastic film of thickness h and modulus E . The latter is strongly bonded to a rigid glass substrate. We consider two extreme cases: the film thickness is larger than the stud radius (Case I, Figure 3) and the film is much thinner than the stud radius (Case II, Figure 4). Figure 5 illustrating our axisymmetric pull-off force apparatus, is given in the section on Materials and Methods, which follows the conclusions.

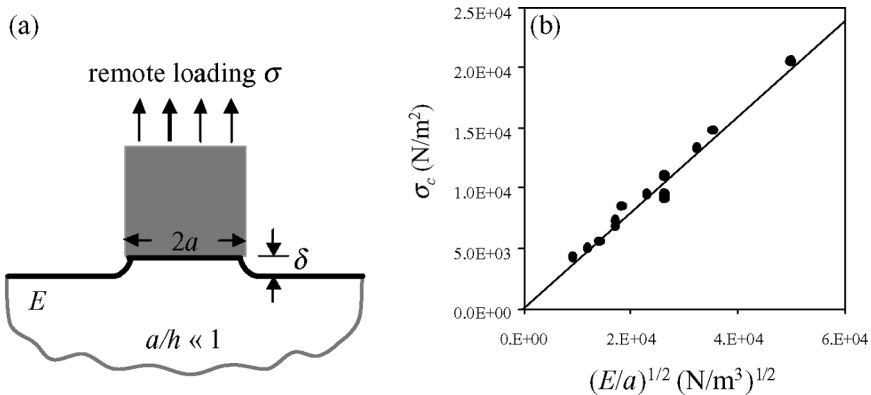


FIGURE 3 (a) Schematic of pull-off of a cylindrical rigid stud from an elastic half space (Case I). (b) Dependence of the critical pull-off stress on $(E/a)^{1/2}$ for $a/h \ll 1$. Both the Young's modulus of the elastic material ($E = 0.77$ to 9.51 Nm^{-2}) and the radius of the smooth-ended glass disk ($a = 3.8$ to 9.0 mm) were varied. All data collapse on a single straight line going through the origin.

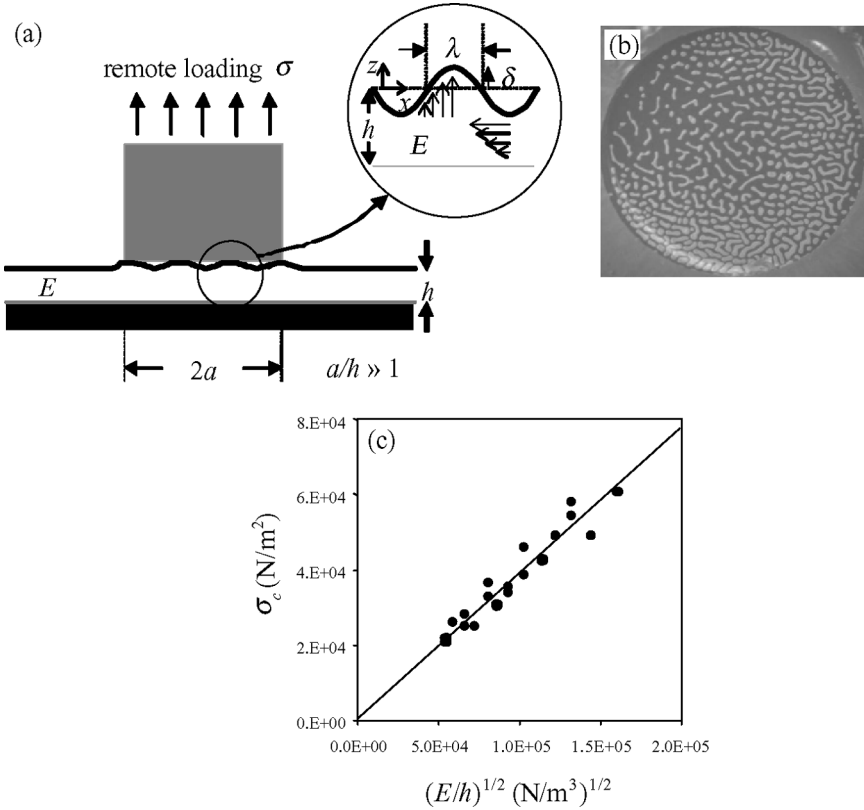


FIGURE 4 (a) Schematic of pull-off of a cylindrical rigid stud from a thin elastic film, showing internal crack propagation with the formation of well-defined interfacial instabilities (Case II). (b) Video micrograph of cavitation bubbles observed during pull-off. The radius of glass disk $a = 3.8$ mm, film thickness $h = 76$ μm , and Young's modulus of the film $E = 2.66$ Nm^{-2} . (c) Dependence of the critical pull-off stress on $(E/h)^{1/2}$ for $a/h \gg 1$. All data collapse on a single straight line passing through the origin.

Case I: Rigid disk on a soft elastic slab ($a/h \ll 1$): It was observed first by Kendall [1] and later by other groups [3, 4, 7, 10–12] that for a rigid disk being pulled from a soft elastic slab, the crack initiates at the periphery of the contact and propagates toward the center (edge crack, Figure 3a). The situation can be analyzed using the overall energy balance approach of Kendall [1] or by the stress intensity approach as was done by Maugis [20]. Maugis considered a Boussinesq [21] stress distribution at the interface of the cylindrical stud and a

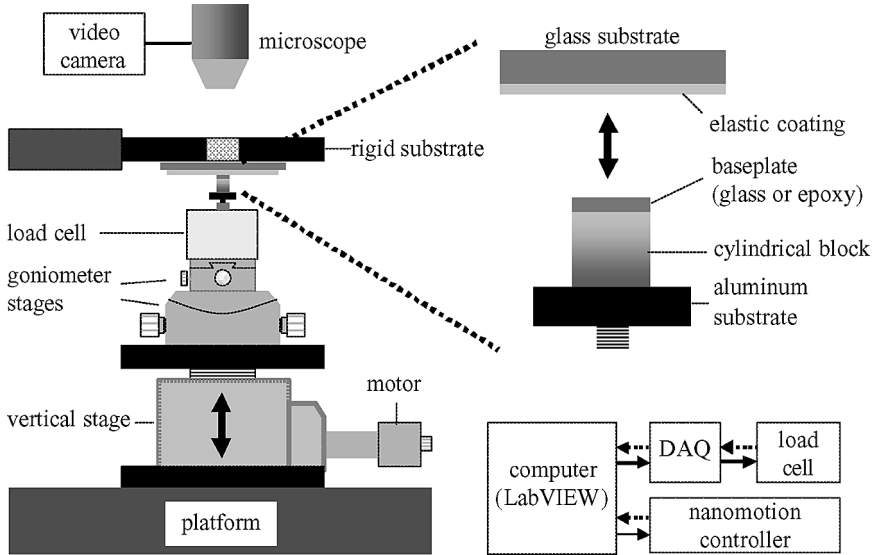


FIGURE 5 Schematic of the axisymmetric pull-off force apparatus. A cylindrical block of PDMS having a thin glass or epoxy baseplate above it is brought into complete contact with a PDMS coating supported on a glass slide. A two-axis goniometer stage allowed accurate adjustment of the axial alignment. A motor connected to a vertical stage could bring the stud in contact with or detach from the elastic coating. A nanomotion controller system allowed control of the vertical displacement, and a load cell mounted on the cylindrical stud allowed measurement of the load using the computer-assisted data-acquisition system. Contact images at the interface between the stud and the coating were viewed using an optical microscope equipped with a CCD video camera and analyzed with motion-tracking software.

semi-infinite half space:

$$\sigma(r) = \frac{F}{2\pi a(a^2 - r^2)^{1/2}}, \quad r < a. \quad (4)$$

Here, F is the force applied on the disk and r is the radial distance. As r approaches a , Equation (4) becomes

$$\sigma(r) = \frac{K_I}{\sqrt{2\pi x}}, \quad x = a - r. \quad (5)$$

The stress thus has an inverse-square-root singularity at the edge with K_I being the stress intensity factor in mode I [$K_I = F/(4\pi a^3)^{1/2}$], which is related to the strain-energy release rate G as

$$G = \frac{K_I^2(1 - \nu^2)}{2E}. \quad (6)$$

where ν is the Poisson's ratio.

Taking the critical strain-energy release rate to be equal to the work of adhesion, *i.e.*, $G_c = W$, the critical pull-off force is

$$F_c = \sqrt{\frac{8\pi\alpha^3WE}{(1 - \nu^2)}}. \quad (7)$$

The critical stress for pull-off can then be expressed as follows:

$$\sigma_c = \sqrt{\frac{8WE}{\pi\alpha(1 - \nu^2)}}. \quad (8)$$

Equation (8) can also be derived from the overall stiffness (k) of the soft elastic slab, which can be obtained by dividing the applied force F with the extension δ [1], *i.e.*,

$$k = \frac{F}{\delta} = \frac{2Ea}{(1 - \nu^2)}. \quad (9)$$

Substitution of Equation (9) in Equation (3) also leads to Kendall's result [Equation (8)], which predicts that the critical pull-off stress scales as $(E/a)^{1/2}$.

Equation (8) was verified experimentally by Kendall [1], for the case of rigid indenters being pulled from soft gelatin blocks, by keeping its modulus constant but by varying its radius.

We performed an elaborate experiment in which rigid glass discs of various radii (3.8 to 9.0 mm) were pulled from thick (13-mm) poly-(dimethylsiloxane) (PDMS) elastomeric blocks of various Young's-moduli ($E = 0.8$ to 9.5 Nm^{-2}). To prevent nonspecific adhesion, the surfaces of the glass disks were modified by reacting them with hexadecyltrichlorosilanes. The critical force (stress) required to pull the rigid cylinders off the elastomeric block was measured with an apparatus built like a probe tack tester (Figure 5; details are in the Materials and Methods section). When the pull-off stress is plotted against $(E/a)^{1/2}$, a straight line is observed, the slope of which yields $W \approx 47 \text{ mJ m}^{-1}$ using Equation (8), which compares favorably with the value of 42–44 mJ m^{-2} obtained from the JKR (Johnson, Kendall, and Roberts) contact mechanics experiments [22] (see Figure 3). (assuming $\nu \sim 0.5$) We also found that Kendall's equation [Equation (8)], derived for a rigid cylinder being pulled from a soft substrate, is perfectly applicable to the case of a soft PDMS cylinder being pulled

off a hard substrate. This is in agreement with the recent analysis of Hui *et al.* [23], which shows that for an edge crack, both these cases yield approximately similar results. It is thus more appropriate to describe the general situation as [13]

$$\sigma_c = \sqrt{\frac{8WE^*}{\pi a}}, \quad (10)$$

where the composite modulus (E^*) is given by $1/E^* = (1 - \nu_1^2)/E_1 + (1 - \nu_2^2)/E_2$, and the subscripts 1 and 2 represent the substrate and the cylinder, respectively.

Gent [24] derived a similar equation for the adhesive fracture of a thick slab of rubber using the energy criterion of the fracture proposed by Rivlin and Thomas [25]. According to Gent's presentation of the Rivlin and Thomas model, the relationship between W and the strain energy density (W_b) for a thick slab of rubber is $W \cong \pi c W_b$, c being the length of the debond zone. For an adhesive of elastic modulus E , $W_b \cong \sigma_c^2/2E$, which, in conjunction with the Rivlin–Thomas equation yields.

$$\sigma_c = \sqrt{\frac{2WE}{\pi c}}. \quad (11)$$

Gent realized that for circular contact, the nonuniform stress state at the interface needs to be taken into account. When appropriate corrections are made, the exact form of Equation (10) can be derived using the Gent–Rivlin–Thomas approach.

Case II: Rigid stud on a thin elastic film ($a/h \gg 1$): When the thickness of the film is smaller than the radius of the cylindrical stud ($a/h \gg 1$), it cannot undergo a sufficient amount of lateral contraction. Gent [24] derived an expression for the pull-off stress in such constrained system using the Rivlin and Thomas relationship between work of fracture and the strain-energy density (W_b), which for a thin slab of rubber is $W \cong h W_b$, h being the thickness of the rubber slab. Using $W_b \cong \sigma_c^2/2E$, Gent obtained

$$\sigma_c = \sqrt{\frac{2WE}{h}}. \quad (12)$$

Kendall's [1] version of Equation (12) has the term bulk modulus instead of elastic modulus. However, the proper way to derive the expression for the pull-off stress is to take into account the hydrostatic stress state in the film, which leads to the formation of cavitating bubbles (internal crack, Figure 4a) at the interface. Cavitation bubbles of the types shown in Figure 4b were observed by other authors as well

[26–29]. However, it has only been established recently [30–33] that these bubbles arise because of adhesion-induced elastic instability in the film. These bubbles have well-defined spacing (wavelength λ) that scales linearly with the film thickness [30–33]. The wavelength of this instability can be obtained by minimizing the total energy of the system with respect to a surface perturbation mode of wavelength λ . By ignoring the adhesion energy, which to the first-order approximation is independent of λ , the total energy \bar{U}_T (energy/area) consists of the elastic strain energy (\bar{U}_E) and the surface energy (\bar{U}_S):

$$\bar{U}_T \sim Eh \left[\left(\frac{\partial u_z}{\partial x} \right) + \left(\frac{\partial u_x}{\partial z} \right) \right]^2 + \gamma \left(\frac{\partial u_z}{\partial x} \right)^2, \quad (13)$$

where u_x and u_z are the components of the displacement field in the x and z directions (a local Cartesian coordinate is denoted in the inset of Figure 4a). Taking the characteristic length scales as λ and h along the x and z axes ($x \sim \lambda$ and $z \sim h$), and considering that the maximum surface displacement in the z direction is on the order of the amplitude of the perturbation ($u_z \sim \delta$), the maximum displacement along the x direction can be obtained from the incompressibility condition ($\partial u_x / \partial x + \partial u_z / \partial z = 0$), *i.e.*, $u_x \sim \delta \lambda / h$. Minimizing \bar{U}_T with respect to λ yields $\lambda \sim h [1 + \gamma / (Eh)]^{1/4}$ [34]. Because the term $\gamma / Eh \ll 1$, we have the result $\lambda \sim h$ (the exact treatment of the problem, as provided by Shenoy and Sharma, can be found in References [30] and [32]). Using this relationship between λ and h , the net elastic energy of the thin film can be written as

$$U_E = \bar{U}_E \times (\pi a^2) \sim \frac{E \delta^2 a^2}{h}. \quad (14)$$

Substituting Equation (14) into Equation (1) leads to the expression for the stiffness of the film:

$$k \sim \frac{a^2 E}{h}. \quad (15)$$

Equation (15), in conjunction with Equation (3), yields the following expression for the critical pull-off stress:

$$\sigma_c \sim \sqrt{\frac{WE}{h}}. \quad (16)$$

Equation (16) is a simplified version of an expression presented earlier by Webber *et al.* [10], who used the more exact form of the elastic energy in the film as provided by Shenoy and Sharma [30, 32, 35, 36].

Considering only a single Fourier mode of interfacial perturbation, $u_z(x) = \delta \cos(2\pi x/\lambda)$, the expression for the elastic energy of the film becomes [36]:

$$U_E = \frac{A^* \pi E \delta^2}{3h} \frac{(2\pi h/\lambda)[1 + \cosh(4\pi h/\lambda) + 2(2\pi h/\lambda)^2]}{2[\sinh(4\pi h/\lambda) - 4\pi h/\lambda]}, \quad (17)$$

where A^* is the actual area of contact. For an incompressible film of low surface energy, it is shown [30–32] that the total energy is minimized when the wavenumber at the perturbed configuration scales as $2\pi h/\lambda = 2.12$; *i.e.*, $\lambda \sim 3h$. Because our case closely meets these conditions ($\nu \sim 0.5$, $\gamma/Eh \ll 1$), the expression for the elastic energy of the film can be simplified by inserting $2\pi h/\lambda = 2.12$ in Equation (17), *i.e.*,

$$U_E = 1.63 \frac{A^* E \delta^2}{h}. \quad (18)$$

The simulations of Sarkar *et al.* [35, 36] show that the fractional contact area ($A^*/\pi a^2$) remains constant at ~ 0.5 (for details, see Reference 35); *i.e.*, $A^* \cong \pi a^2/2$. The theoretical expression for the stiffness of the thin elastic film is then determined by substituting Equation (18) into Equation (1):

$$k = 5.12 \frac{a^2 E}{h}. \quad (19)$$

Now we obtain the resultant pull-off force as

$$\sigma_c = \sqrt{\frac{3.3WE}{h}}. \quad (20)$$

We performed pull-off force measurements with cylindrical rigid studs of different radius (3.8–9 mm) from PDMS films of thicknesses ranging from 50 to 900 μm and Young's moduli ranging from 0.8 to 9.5 Nm^{-2} . For these thin films, instabilities appeared at the interface much like those reported in References 10, 31, and 33. The pull-off stress varied linearly with $(E/h)^{1/2}$ (see Figure 4c), from the slope of which W is estimated to be 47 mJ m^{-2} using Equation (20), which is in good agreement with the values (42–44 mJ m^{-2}) obtained from JKR contact-mechanics studies [22].

There is another interesting perspective to consider. Debonding of elastic films occurs *via* growth of cavities that are laterally separated by $3h$. With further increase in the force, these periodic wavy patterns elongate in the normal direction, leading to fully developed instabilities with columnar structures. It has been proposed by Sarkar *et al.*

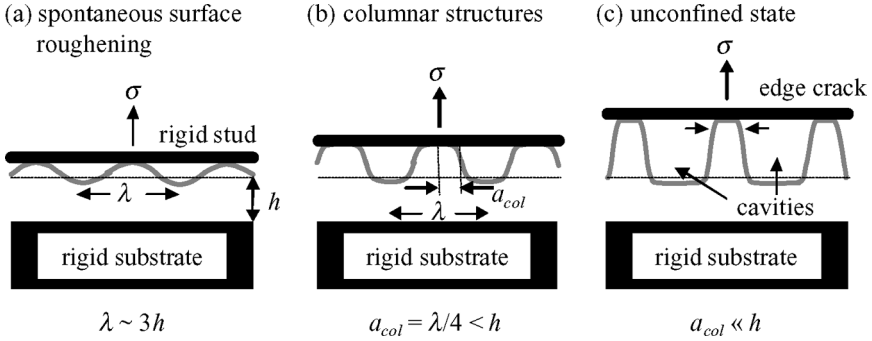


FIGURE 6 Illustration of the pathway of debonding for initially confined geometry, *i.e.*, for $a/h \gg 1$: (a) Initial instability patterns with $\lambda \simeq 3h$. (b) Debonding in the form of columnar structures within the contact area. Here a_{col} represents the contact radius of a single column. At this stage, a_{col} can be assumed to be a quarter of the wavelength of instabilities because $A^*/A \simeq 0.5$. (c) An unconfined state. As columns stretch, stress concentrations occur at the edge of the columns, leading to the decrease in the contact area (peeling mode).

[35] that debonding of a single column proceeds by decreasing the area of contact with increasing force until a catastrophic “snap-off” of the bridging column occurs. In other words, the mode of failure of a single column is that of edge crack propagation, as illustrated in Figure 6. This situation is similar to the case of a soft cylinder being pulled off a rigid half space, for which Kendall’s equation [Equation (8)] applies. Here, we consider a single columnar structure of radius $\sim \lambda/4$ as illustrated in Figure 6b. Taking the effective radius of contact of the cylindrical stud in Equation (8) to be $3h/4$ (assuming $\lambda \sim 3h$), we estimate the pull-off stress to be

$$\sigma_c \cong 2\sqrt{\frac{WE}{h}}. \quad (21)$$

Equation (21) shows that the critical pull-off stress scales as $(E/h)^{1/2}$ with a prefactor not too different from that in Equation (20). It is important to point out that Yang and Li [4] recently derived the expressions for the pull-off force by considering different types of slip boundary conditions at interfaces. Among these relations, the equation [see Equation (22)] that was derived on the assumption that both the stud/film and the film/substrate interfaces are free of friction predicts the pull-off stress to be proportional to $(E/h)^{1/2}$, *i.e.*,

$$\sigma_c = \frac{F}{\pi a^2} = 1.64\sqrt{\frac{WE}{h}}. \quad (22)$$

Conversely, if slippage occurs only at the stud/film interface, and not at the film/substrate interface, the pull-off force varies inversely as $h^{3/2}$. We have not fully explored the implications of these predictions in the context of our model studies. However, it is important to note that the Yang and Li [4] did not consider elastic instability at the interface. It will be interesting to explore experimental systems in which separation does not proceed *via* instability but by slippage of the type envisaged by Yang and Li.

A Special Case of Two Confined Films

There is yet another interesting scenario to consider. It appears (G. W. Swain, personal communication) that certain biofoulants, *e.g.*, barnacles, could have a thin rubbery region underneath the harder adhesive baseplate. The failure mechanism of such a composite baseplate from a thick elastomer can still be described by Equation (8), because the latter is more compliant than its composite counterpart. However, when the adhesive is in contact with a thin elastomer, the situation changes as the compliance of the entire system and the resulting instability depend on the modulus and thickness of the rubbery adhesive as well as those of the elastomeric film (Figure 7). The general treatment of the instability at the interface of two confined films has been carried out previously by Sarkar *et al.* [37].

Here we analyze the situation using a simple energy-balance approach. Ignoring the contributions of the surface and adhesion energies, the total elastic energy in film 1 and 2 for an interfacial perturbation [see Equation (13)] of wavelength λ can be written as

$$\bar{U}_T \sim E_1 h_1 \delta_1^2 \left(\frac{1}{\lambda} + \frac{\lambda}{h_1^2} \right)^2 + E_2 h_2 \delta_2^2 \left(\frac{1}{\lambda} + \frac{\lambda}{h_2^2} \right)^2, \quad (23)$$

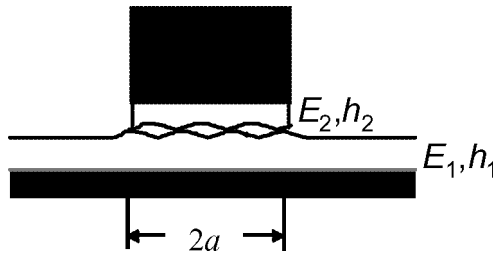


FIGURE 7 Instability at the interface of two confined films depends on the modulus and thickness of both the films.

where δ_1 and δ_2 are the amplitudes of the perturbations in the films 1 and 2, respectively. To determine the wavelength of interfacial perturbations, \bar{U}_T has to be minimized with respect to λ . However, before such minimization is attempted, we need to find a relationship between δ_1 and δ_2 , which can be accomplished by balancing the hydrostatic stresses in the films. Under the lubrication approximation [33],

$$P_0 + \frac{E_1 \delta_1 \lambda^2}{h_1^3} \exp\left(\frac{2\pi x i}{\lambda}\right) = P_0 + \frac{E_2 \delta_2 \lambda^2}{h_2^3} \exp\left(\frac{2\pi x i}{\lambda}\right) \text{ or } \frac{E_1 \delta_1}{h_1^3} \sim \frac{E_2 \delta_2}{h_2^3}, \quad (24)$$

where P_0 is the average hydrostatic stress in the films. With the assumption that the wavelength of instability is significantly larger than the thicknesses of both the films, we minimize \bar{U}_T with the help of Equations (23) and (24) to yield

$$\lambda \sim \left(\frac{E_1 h_2^7 + E_2 h_1^7}{E_1 h_2^3 + E_2 h_1^3} \right)^{1/2}. \quad (25)$$

Substitution of Equations (23)–(25) in Equation (3) yields the expression for the pull-off stress as follows:

$$\sigma_c \sim \left(\frac{WE_1 E_2 (E_1 h_2^7 + E_2 h_1^7)^{1/2}}{(E_1 h_2^3 + E_2 h_1^3)^{3/2}} \right)^{1/2}. \quad (26)$$

Note that Equation (26) reduces to Equation (16) for $E_1 = E_2$ and $h_1 = h_2$. In other words, the expression for the pull-off force for two fully confined thin films of identical modulus and thickness is the same as that of one film from a rigid support. For other situations, the pull-off force depends on both the modulus and thickness in a nonlinear way. A detailed account of these studies will be published elsewhere.

Effective Stiffness for a Pseudo-foulant on an Elastic Film

We now consider the effect of stiffness of the pseudo-foulant, which is in contact with a thin elastic film (Figure 8). When the elastic block bonded to the flexible baseplate is stretched in the normal direction, the latter may undergo bending (as illustrated in Figure 2b) due to nonuniform stress distribution at the interface. In the extreme limits of either the baseplate being infinitely rigid or the elastic block being of infinite modulus, bending in the baseplate would be negligible. However, for a thin baseplate and a deformable elastic block, a Boussinesq-type [21] nonuniform stress at the interface can cause bending in the baseplate.

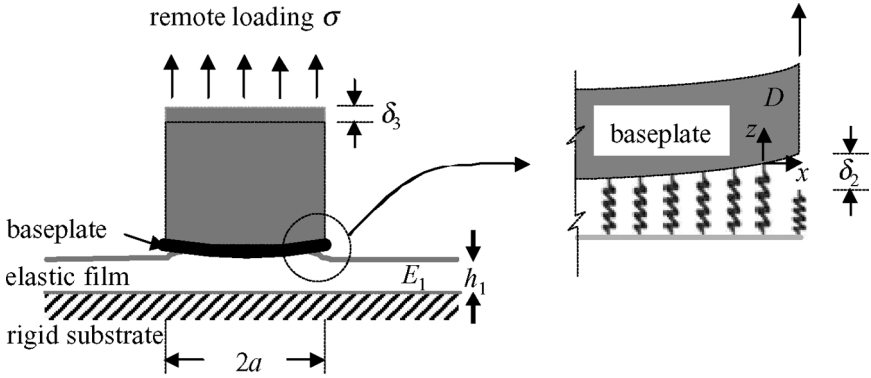


FIGURE 8 Schematic of pull-off of a flexible pseudo-foulant from an elastic film. Adhesion of the flexible baseplate on the elastic film is treated as a beam on elastic foundation model because of the bending effect.

The force (P , per unit length) acting on the edge of the bent plate can be estimated by estimating the effective moment of the force due to distributed Boussinesq stress as

$$P(2\pi a)a \cong 2\pi \int_0^a \sigma(r)r^2 dr. \tag{27}$$

Using the expression for $\sigma(r)$ as in Equation (4), we find $P \sim F/a$. This force can be equated with that arising from the profile of the bent plate as

$$P = D \frac{\partial^3 u_z}{\partial x^3}, \tag{28}$$

where u_z is the component of the displacement field in the z direction (Figure 8), and D is the bending stiffness (or flexural rigidity) of the baseplate [38]

$$D = \frac{E_2 h_2^3}{12(1 - \nu_2^2)} \tag{29}$$

The bending of the baseplate is, however, strongly coupled to the deformation of the thin elastic film below it. This elastic coupling determines the length over which stress decays from the edge of the contact towards the center. For a plate in contact with a thin confined film, this distance is given by the following expression [39, 40]:

$$\xi \sim \left(\frac{D h_1^3}{E_1} \right)^{1/6} \tag{30}$$

By taking $u_z \sim \delta_2$ and $x \sim \xi$, Equation (28) can thus be analyzed at the scaling level as, $P \sim F/a \sim D\delta_2/\xi^3$. Next, assuming that the crack initiates at the edge of contact, we consider the elastic strain-energy release rate due to the bending of a plate [41]:

$$\bar{U}_2 = D \left(\frac{\partial^2 u_z}{\partial x^2} \right)^2. \quad (31)$$

Equating \bar{U}_2 to W , the work of adhesion, we find $W \sim D\delta_2^2/\xi^4$. Now, combining these expressions for P , W , and ξ , we get

$$\left(\frac{F}{a} \right)^2 \sim \frac{WD^{2/3}E_1^{1/3}}{h_1}. \quad (32)$$

In terms of the remote stress, Equation (32) becomes

$$\sigma_c = c \left[\frac{WD^{2/3}E_1^{1/3}}{h_1 a^2} \right]^{1/2}, \quad (33)$$

where c is a numerical prefactor to be determined experimentally. Although the effect of the baseplate on the adhesive pull-off force cannot be studied independently of the elastomeric block above it, Equation (33) shows that its size and rigidity should have profound effects on the measured forces.

The model system consists of a thick elastomeric rubber cylinder (thickness 5 mm and Young's modulus ~ 1.5 MPa) bonded to thin flexible plates of either glass or epoxy of flexural rigidity ranging from 0 to 5.5 Nm. The force needed to pull these cylinders from thin PDMS films were measured with a home-built device (see the section on Materials and Methods for details). To achieve the condition $a/h_1 \gg 1$, we used the contact radius of the cylinder in the range of 3.8–9 mm and the thickness of the PDMS film in the range of 50–900 μm .

Figures 9 and 10 summarize the pull-off stresses as a function of the thickness and modulus of the PDMS film as well as the rigidity of the base plate. For an effectively rigid baseplate ($D = 5.5$ Nm), the pull-off stress decreases with the film thickness but increases with the modulus as predicted by Equation (20). These data can be combined to show that the pull-off stress varies as $(E/h_1)^{1/2}$, which has been discussed in an earlier section (see Figure 4). Conversely, in the absence of the baseplate ($D = 0$), the pull-off stress does not depend on the film thickness (see also Figure 3). When D is in between these extremes, the

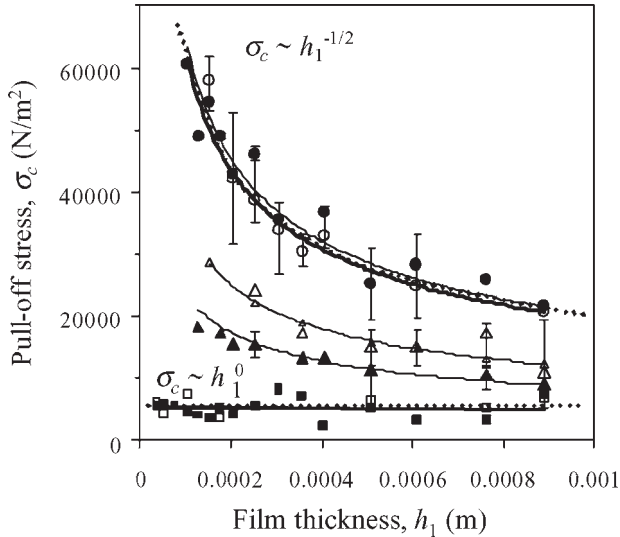


FIGURE 9 Experimental pull-off stresses (σ_c) for various flexural rigidities (D) and the thickness (h_1) of the PDMS film with $E_1 = 2.7$ MPa: $D = 5.47$ Nm (\circ), $D = 5.00 \times 10^{-1}$ Nm (\bullet), $D = 3.70 \times 10^{-3}$ Nm (\triangle), $D = 8.34 \times 10^{-4}$ Nm (\blacktriangle), $D = 3.04 \times 10^{-7}$ Nm (\square), and $D = 0$ Nm (\blacksquare). The dashed lines represent two extreme limits and the solid lines are predictions based on Equation (34).

pull-off stress moderately depends on both the thickness and modulus of the PDMS films.

Total Critical Pull-Off Stress

In the absence of a rigorous theoretical framework, we perceive the behavior of our model system with an *equivalent mechanical approach*, in which individual elastic bodies of the system are represented by mechanical springs. In such a case, we may consider that the elastic deformation of each component (elastic film, flexible baseplate, and elastic block) contributes to the composite (or total) stiffness of the system. The total stiffness of the system (s) is due to two springs in series: one is that of the elastic film (s_1) and the other (s_{eff}) is due to the baseplate coupled to the elastic block. As such, the stiffness of the coupled system can be expressed using a harmonic equation.

In the pseudo-foulant, the baseplate and elastic block are strongly bonded to each other, the effective stiffness of which depends on various factors. In the limit that the baseplate is infinitely rigid, the stress distribution will be Boussinesq as it is at the elastic block/baseplate

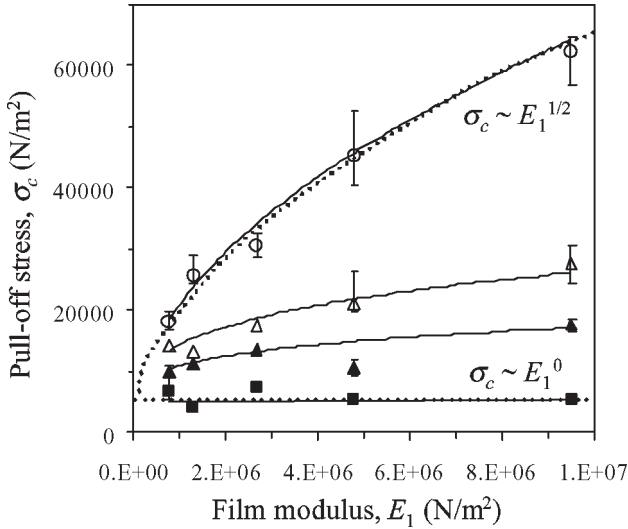


FIGURE 10 Experimental pull-off stresses (σ_c) for various flexural rigidities (D) as a function of the elastic modulus of the film (E_1) with $h_1 = 350 \mu\text{m}$: $D = 5.47 \text{ Nm}$ (\circ), $D = 3.70 \times 10^{-3} \text{ Nm}$ (\triangle), $D = 8.34 \times 10^{-4} \text{ Nm}$ (\blacktriangle), and $D = 0 \text{ Nm}$ (\blacksquare). The dashed lines represent two extreme limits and the solid lines are predictions based on Equation (34).

interface. However, this stress profile cannot be felt by the baseplate/film interface. This problem then is closer to a rigid block being pulled off a soft substrate, in which case the interfacial stress profile is determined by the mechanical properties and the thickness of the substrate. When the baseplate is soft, a Boussinesq-like stress profile should develop at the plate/film interface. This problem, then, is closer to a soft cylindrical block being pulled off a rigid or a soft substrate. As described for a rigid baseplate, the effect of the stiffness of the elastic block indeed becomes negligible, whereas it becomes prominent when the baseplate is very soft. These observations can be treated *empirically* by taking the effective stiffness of the elastomeric block bonded to a baseplate as the arithmetic sum of the stiffnesses of the individual components, *i.e.*, $s_{\text{eff}} = S_2(\text{flexible baseplate}) + S_3(\text{elastic block})$. Because we have considered the behavior of the individual elements, we combine their joint behavior by combining Equations (8), (20), and (33) by defining the adhesive stiffness of each element as σ_c^2/W . Thus, the adhesive stiffnesses for the elements described in Equations (20), (33), and (8) are $s_1 = 3.3 E_1/h_1$, $s_2 = c^2 D^{2/3} E_1^{1/3}/h_1 a^2$, and $s_3 = 3.4 E_3/a$, respectively. These elements are combined as $(1/s) = (1/s_1) + [1/(s_2 + s_3)]$ to

yield the net adhesive stiffness when all the elements are active [see Equations (34) and (35)]:

$$\frac{W}{\sigma_c^2} = \left[\frac{1}{(3.3 E_1/h_1)} + \frac{1}{(c^2 D^{2/3} E_1^{1/3}/h_1 a^2) + (3.4 E_3/a)} \right] \text{ for } a/h_1 \gg 1 \quad (34)$$

$$\frac{W}{\sigma_c^2} = \left[\frac{1}{(3.4 E_1/a)} + \frac{1}{(c^2 D^{2/3} E_1^{1/3}/h_1 a^2) + (3.4 E_3/a)} \right] \text{ for } a/h_1 \ll 1. \quad (35)$$

Note that all the limiting cases [*i.e.*, Equations (8), (10), (20), and (33)] can be obtained from this equation quite readily. For example, when the baseplate is infinitely rigid (*i.e.*, $D \rightarrow 0$), the equation for the pull-off stress is simplified to either Equation (20) or Equation (8). As the baseplate becomes very compliant (*i.e.*, $D \rightarrow \infty$), the stiffness of the elastic film and/or that of the elastic block determine the system stiffness.

Next, we investigate if Equations (34) and (35) can be used to summarize all the pull-off force data in one master plot by fitting the one adjustable parameter c . To achieve this objective, we employed 84 sets of pull-off force data corresponding to twelve different film thicknesses (h_1), five different film moduli (E_1), five different baseplate radii (a), and six different rigidities of the baseplate (D), including the data shown in Figures 9 and 10. Using the method of least squares, the unknown prefactor c in Equations (34) and (35) is found to be 13.7 with a correlation coefficient of 0.97. Using this value of c , the pull-off stresses as predicted by Equations (34) and (35) are compared with the measured values (Figure 11).

Although the correlation reported in Figure 11 is excellent, the large numerical value of c (13.7) needed in Equations (34) and (35) is considerably larger than the value (~ 3) expected if all the numerical prefactors were retained in the derivation of Equations (34) and (35). The discrepancy therefore raises the concern that some important mechanisms of debonding might not have been properly understood, even though Equations (34) and (35) seem to be consistent with the experimental data in terms of the materials and geometric properties of the system. The obvious point that comes to our mind is the assumption that the crack opens from the edge and that this opening is fracture-toughness controlled. Experimentally, we know that this is not necessarily the case, because in most of the instances the crack nucleates by cavitation at the interface. These factors lead to several

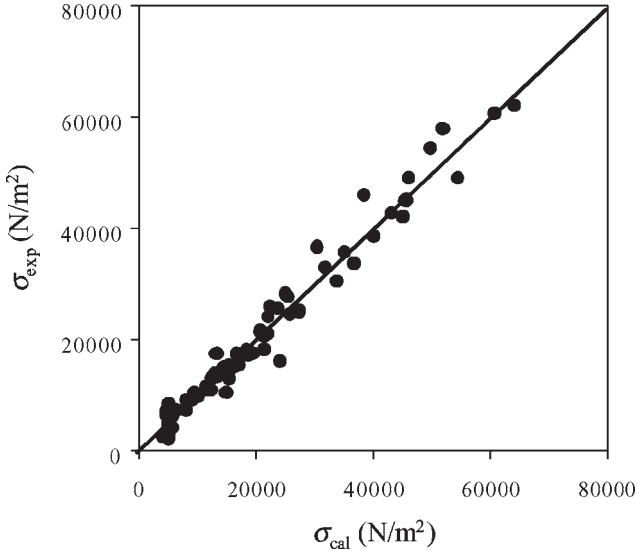


FIGURE 11 The master curve describing the correlation between the predicted [Equations (34) and (35)] and measured pull-off stresses.

complications associated with the analysis of the problem. First, complication results from insufficient knowledge of the hydrostatic state of the film; second, it is not quite clear whether the process of crack initiation is controlled by work of adhesion or by the cohesive stress. Proper analysis of this problem would require rigorous solutions of the elastic field equations with the unfortunate loss of the simplicity of the method presented here. Although such a rigorous analysis would be warranted for a complete understanding of the problem, the success achieved here in being able to present all the pull-off stress data under one master equation leads us to believe that this protocol would be of value in estimating the removal forces of complex fouling organisms.

There could yet be other important applications of the methodologies developed here. Recently, a significant amount of research is being directed to trying to mimic the adhesive pads of animal and insects, because much can be learned from the way they optimize adhesion based on elastic and geometric properties [34, 42–50]. The adhesive pads of many of these species are endowed with fine fibrillar structures [42, 45], which can adhere to a surface by van der Waals force alone. There are reasons to believe that the high adhesive properties of these adhesive pads result from the collective behaviors of the individual fibrils. Consider a flat-ended fiber of

length L , radius a , and elastic modulus E_1 in contact with a flat surface. When such a fiber is pulled a surface, it detaches when the detachment stress reaches the value given by Equation (10), *i.e.*, $\sigma \sim \sqrt{WE_1/a}$. However, the fiber stores some extra elastic energy, which is not recovered when it detaches from the substrate. This energy dissipation per unit area is $\sigma^2 L/E_1 = W(L/a)$. Thus, as the effective fracture energy is enhanced by the aspect ratio of the fibril L/a , it makes sense to synthesize artificial adhesives with long aspect ratio [23, 34, 48, 50]. There is, however, a severe practical limitation to this approach. Long fibrils collapse laterally by adhesion-induced buckling [48]. A possible way to overcome this problem is to avoid very long fibrils, but modifying its tip with a thin rigid baseplate followed by coating it with a soft polymer (of thickness h and modulus E_2). If the baseplate is effectively rigid, the detachment stress would be given by Equation (20), *i.e.*, $\sigma \sim \sqrt{WE_2/h}$, and the energy dissipation per unit area would be $\sigma^2 L/E_1 = W(E_2/E_1)(L/h)$. Taking $E_1 = E_2$, the energy dissipation is $W(L/h)$. The new aspect ratio is now L/h , which can be made as large as needed by decreasing h without having to use long fibrils (*i.e.*, high L/a), we may ask how thick the baseplate has to be so that it behaves effectively rigidly. The answer to this question can be obtained by setting $c^2 D^{2/3} E_2^{1/3} / h a^2 > 3.4 E_1 / a$ [Equations (8) and (33)], which translates to a lower value of $D \sim 0.0025 E_1 (h a)^{3/2}$. Taking E_1 to be about 1 MPa, $h \sim 1 \mu\text{m}$ and $a \sim 10 \mu\text{m}$, this lower value of D is estimated to be only about 10^{-14}Nm . In other words, very flexible baseplates in a macroscopic sense would behave like a rigid plate at this scale.

It should also be pointed out that the relationship between the pull-off stress and the modulus of the elastomer, as embodied in Equations (10) and (16), is strictly applicable for cases where the work of adhesion is independent of molecular weight. In the particular cases reported in this article, W is independent of molecular weight because the main interaction is *via* dispersion forces. However, if the polymer chains interact with the counter surface *via* nondispersion forces, W can be a strong function of molecular weight (M) [51–56]. In the literature, W has been reported to depend on M as $W \sim M^\alpha$ with α ranging from 1/2 to 1. As the modulus varies inversely with the molecular weight, W is expected to vary with E as $W \sim E^{-1/2}$ or $W \sim E^{-1}$. In these situations, the pull-off stress may have a weak dependence on modulus, *i.e.*, $\sigma \sim E^{1/4}$, or may not depend on modulus at all. There are also possibilities for viscoelastic relaxations either in the bulk [6, 7] or at the interface [55, 56], which would have additional effects on the relationship between the pull-off stress and molecular weight.

III. CONCLUDING REMARKS

The experimental results reported here illustrate the roles of mechanical and geometric properties of both the adherents and adhesives in their detachment forces. The basic results of this work confirm the previous findings of Kendall [1] and other authors [3, 4, 10]. The main result of this work is to introduce a thin adhesive baseplate under a soft stud and to demonstrate the transition from the unconfined (soft) to confined (hard) adhesion by manipulating its flexural rigidity. It is hoped that these results will be of value in understanding the adhesive behavior of fouling organisms to polymer-coated ship hulls, because these organisms exhibit adhesive baseplates of various rigidities. The classification of fouling behavior, which is normally done with such terminologies as “soft” and “hard” either because of the variation of species or different stages of maturation, may now be done more quantitatively by taking into consideration the size of the species and the material properties of the whole system.

Materials and Methods

Preparation of elastic coatings of PDMS bonded to rigid substrates: Elastomeric films and slabs were made of poly-(dimethylsiloxane) using the following procedure. Glass microscope slides ($25 \times 75 \times 1$ mm, Fisher Scientific, Pittsburgh, PA, USA) were cleaned by immersion in hot piranha solution (70% H_2SO_4 + 30% of a 50% solution of H_2O_2) for 30 min, and then thoroughly rinsed with purified water and dried under pure nitrogen flow. They were further subjected to oxygen plasma treatment in a plasma cleaner (model PDC-32G, 100 W, Harrick Plasma, Ithaca, NY, USA) at a pressure of 0.2 Torr for 45 s at low power setting. One set of these glass slides was used as rigid substrates. The other set was coated with a self-assembled monolayer (SAM) of hexadecyltrichlorosilane (United Chemicals Technologies Inc., Bristol, PA) using a method described elsewhere [22]. The ingredients for preparing PDMS elastomers (obtained as gifts from Dow Corning Corp., Midland, MI) consisted of four parts, vinyl-terminated PDMS oligomers ($\text{H}_2\text{C}=\text{CH}(\text{Si}(\text{CH}_3)_2\text{O})_n\text{Si}(\text{CH}_3)_2\text{CH}=\text{CH}_2$) of different molecular weights, the platinum catalyst (Syloff 4000), the maleate inhibitor (Syloff 7694), and the methylhydrogen siloxane cross-linker (Syloff 7678: $(\text{H}_3\text{C})_3\text{O}-(\text{SiHCH}_3\text{O})_p(\text{Si}(\text{CH}_3)_2\text{O})_q\text{Si}(\text{CH}_3)_3$, M_n and $M_w = 3.5$ and 7.5 kg/mol, respectively) [13, 22]. The use of oligomers of different molecular weights provided coatings of different Young's moduli ($0.77\text{--}9.51\text{Nm}^{-2}$). These ingredients were mixed thoroughly and

degassed for 30 min in a vacuum. The PDMS specimens bonded to the glass substrate were prepared by first pouring the homogeneous mixture on the cleaned and plasma-oxidized glass slide and then covering it by the glass slide treated with the SAM (serving as the easy-release material). Spacers of various thicknesses were inserted between the two glass slides to achieve uniform and controlled coating thickness. After the mixtures were cured at 120°C for 50 min in a preheated convection oven, the glass slide with the SAM coating was carefully peeled off, leaving only a flat coating on the glass substrate. Further details of the preparation the PDMS coatings are described elsewhere [13, 30, 33].

Preparation of cylindrical blocks of PDMS bonded to rigid aluminum substrates:

The cylindrical blocks of silicone elastomers (thickness 5 mm) were prepared using a 10:1 mixture of PDMS prepolymer and curing agent (Sylgard 184, Dow Corning Corp., Midland, MI). A mixture of these two solutions was degassed for 30 min in a vacuum, poured onto a flat-bottomed polystyrene Petri dish, and cured in an oven at 65°C for 2 h. Then, a slab of a cross-linked silicone elastomer was carefully removed from the Petri dish, from which cylindrical blocks (radius 3.8–9 mm) were cut out with sharp cylindrical steel punches. The cylindrical block was placed on the end of a flat circular aluminum disk, the other end of which contained a screw to fasten it to a load cell. To secure good bonding between the PDMS and aluminum, both were plasma-oxidized using the Harrick plasma cleaner. After gently pressing them together, they were stored under atmospheric condition for at least 1 day before use.

Rigid glass disks and preparation of thin flexible epoxy baseplates:

Baseplates used in these experiments were thin plates made of either glass or epoxy. Borosilicate glass disks (thickness 1.1 mm, Swift Glass Company Inc., Elmira, NY, USA) of different radius (3.8–9 mm) were chosen as rigid studs, the flexible rigidity of which was 5.47 Nm. The epoxy system used was composed of three components, Epon 828 base resin with an epoxide equivalent weight 187.5 (Resolution Performance Products, Houston, TX, USA), Jeffamine[®] T-403 epoxy curing agent (Huntsman Corp., Salt Lake City, UT, USA), and Accelerator 399 (Huntsman Corp., Salt Lake City, UT, USA). The base resin, curing agent, and accelerator were mixed thoroughly with the mass ratio of 100:42:5 followed by degassing *via* centrifugation (8000 rpm for 6 min). Baseplates were fabricated by casting the mixture between two hydrophobic glass slides, which had previously been coated with hydrocarbon SAM. The epoxy baseplates with different

thicknesses (1180, 230, 140, and 10 μm) were controlled with spacers of different heights that were placed between the two slides. The epoxy mixture was cured at 80°C for 2 h and then at 125°C for 3 h. This process produced the cured epoxy that yielded an elastic modulus 3.12 GPa. After complete cure of the epoxy, the flat sheets of epoxy were carefully detached from the two hydrophobic glass slides and were cut into circular shapes (radius 3.8–9 mm). The resulting flexural rigidities of the epoxy baseplate (5.00×10^{-1} , 3.70×10^{-3} , 8.34×10^{-4} , and 3.04×10^{-7} Nm) were estimated using Equation (29) with a Poisson's ratio of 0.38 for the cured epoxy resin.

Preparation of model foulants: Model foulants (consisting of a cylindrical elastomeric block bonded to a baseplate of either glass or epoxy) were prepared using the following procedure. The glass disks were first cleaned by immersion in hot piranha solution for 30 min. Then, the glass disks, epoxy baseplates, and cylindrical PDMS blocks were rinsed thoroughly in distilled, deionized water and blow dried in nitrogen gas. Both the glass disks and epoxy baseplates were bonded to the cylindrical blocks by first plasma oxidizing only the bonding surfaces and then contacting them with gentle pressure. They were allowed to stand overnight until good bonding between them was achieved. The glass disk was then coated with a hydrocarbon SAM. The contact angle of water on the SAM covered glass surface was about 110°.

Axisymmetric pull-off apparatus: Figure 5 shows the schematic of our home-built apparatus used to measure the forces to pull off a flat-ended cylindrical stud (*i.e.*, model foulant) from a soft elastic coating that was deposited on a rigid glass substrate. This apparatus allows precise measurements of the force and displacement and enables simultaneous observation of the interface during the pull-off process. This instrument was built in the image of that used by Creton *et al.* [6, 7] in their probe tack studies. The PDMS-coated glass slides were strongly attached to a rigid steel plate with a commercial double-stick tape. The steel plate had a cylindrical hole at the center, which enabled optical viewing of the interface through the transparent glass substrate. The cylindrical stud bonded to a rigid aluminum plate was mounted through a load cell (model L2338, Futek Advanced Sensor Technology, Inc., Irvine, CA, USA) onto a two-axis goniometer stage (Melles Griot Photonics Components, Carlsbad, CA, USA). Careful alignment of the sample on the coating was critical to the measurements of pull-off forces. To achieve accurate axial alignment between the cylindrical stud and the elastic coating, two axis goniometer stages were utilized to adjust alignment

via a precision bubble level, which was placed on the top of the specimen. The cylindrical stud could be moved upward or downward with a nanomotion controller system attached to a vertical translation stage (Melles Griot Photonics Components, Carlsbad, CA, USA). Contact images could be viewed using an optical microscope (Nikon, model SMZ-2T, Mager Scientific, Dexter, MI, USA) equipped with a CCD video camera (Sony, model XC-75, Optical Apparatus Co., Ardmore, PA, USA). After the complete alignment, the cylindrical stud was moved toward the coating until it made complete contact. The measurements of adhesion (normal pull-off) forces were conducted as follows. The contact between the stud and the elastic coating was maintained for 30 min before the stud was pulled off. The contacting stud was retracted from the coating at a constant displacement rate of $1.5\ \mu\text{m/s}$ using a nanomotion controller system. During the debonding process, the load cell allowed the simultaneous acquisition of voltage data, which were converted to force data using a computer-assisted data-acquisition system (model PCI-DAS6035, Measurement Computing Corp., Middleboro, MA, USA) via Lab VIEW software. The maximum pull-off force was transformed into a critical stress by dividing the force by the initial contact area.

ACKNOWLEDGMENT

This work was supported by the Office of Naval Research (ONR). We thank A. Sharma, A. Ghatak, I. Singer and K. Shull for valuable discussions.

REFERENCES

- [1] Kendall, K., *J. Phys. D: Appl. Phys.* **4**, 1186–1195 (1971).
- [2] Griffith, A. A., *Philos. Trans. R. Soc. Lond. A* **221**, 163–198 (1921).
- [3] Ganghoffer, J.-F. and Gent, A. N., *J. Adhes.* **48**, 75–84 (1995).
- [4] Yang, F. and Li, J. C. M., *Langmuir* **17**, 6524–6529 (2001).
- [5] Mowery, C. L., Crosby, A. J., Ahn, D., and Shull, K. R., *Langmuir* **13**, 6101–6107 (1997).
- [6] Lakrout, H., Sergot, P., and Creton, C., *J. Adhes.* **69**, 307–359 (1999).
- [7] Creton, C. and Lakrout, H., *J. Polym. Sci., Part B: Polym. Phys.* **38**, 965–979 (2000).
- [8] Shull, K. R., Flanigan, C. M., and Crosby, A. J., *Phys. Rev. Lett.* **84**, 3057–3060 (2000).
- [9] Crosby, A. J., Shull, K. R., Lakrout, H., and Creton, C., *J. Appl. Phys.* **88**, 2956–2966 (2000).
- [10] Webber, R. E., Shull, K. R., Roos, A., and Creton, C., *Phys. Rev. E* **68**, 021805 (2003).
- [11] Brady, Jr., R. F. and Singer, I. L., *Biofouling* **15**, 73–81 (2000).

- [12] Singer, I. L., Kohl, J. G., and Patterson, M., *Biofouling* **16**, 301–309 (2000).
- [13] Chaudhury, M. K., Finlay, J. A., Chung, J. Y., Callow, M. E., and Callow, J. A., *Biofouling* **21**, 41–48 (2005).
- [14] Callow, M. E., Callow, J. A., Pickett-Heaps, J. D., and Wetherbee, R., *J. Phycol.* **33**, 938–947 (1997).
- [15] Callow, J. A., Crawford, S. A., Higgins, M. J., Mulvaney, P., and Wetherbee, R., *Planta* **211**, 641–647 (2000).
- [16] Becka, A. and Loeb, G., *Biotechnol. Bioeng.* **26**, 1245–1251 (1984).
- [17] Swain, G. W. J. and Schultz, M. P., *Biofouling* **10**, 187–197 (1996).
- [18] Sun, Y. I., Guo, S. L., Walker, G. C., Kavanagh, C. J., and Swain, G. W., *Biofouling* **20**, 279–289 (2004).
- [19] Vaccaro, E. and Waite, J. H., *Biomacromolecules* **2**, 906–911 (2001).
- [20] Maugis, D., *J. Colloid Interface Sci.* **150**, 243–269 (1992).
- [21] Boussinesq, J., *Application des potentiels a l'etude de l'equilibre et du mouvement des solides elastiques* (Gauthier Villars, Paris, 1885).
- [22] Vorvolakos, K. and Chaudhury, M. K., *Langmuir* **19**, 6778–6787 (2003).
- [23] Hui, C.-Y., Glassmaker, N. J., Tang, T., and Jagota, A., *J. R. Soc. Interface* **1**, 35–48 (2004).
- [24] Gent, A. N., *Rubber Chem. Technol.* **47**, 202–212 (1974).
- [25] Rivlin, R. S. and Thomas, A. G., *J. Polym. Sci.* **10**, 291–318 (1953).
- [26] Gent, A. N. and Lindley, P. B., *Proc. R. Soc. Lond. A* **249**, 195–205 (1959).
- [27] Gent, A. N. and Tompkins, D. A., *J. Polym. Sci. Polym. Phys. Ed.* **7**, 1483–1488 (1969).
- [28] Gent, A. N. and Tompkins, D. A., *J. Appl. Phys.* **40**, 2520 (1969).
- [29] Kaelble, D. H., *Trans. Soc. Rheol.* **15**, 275–296 (1971).
- [30] Ghatak, A., Chaudhury, M. K., Shenoy, V., and Sharma, A., *Phys. Rev. Lett.* **85**, 4329–4332 (2000).
- [31] Mönch, W. and Herminghaus, S., *Europhys. Lett.* **53**, 525–531 (2001).
- [32] Shenoy, V. and Sharma, A., *Phys. Rev. Lett.* **86**, 119–122 (2001).
- [33] Ghatak, A. and Chaudhury, M. K., *Langmuir* **19**, 2621–2631 (2003).
- [34] Chung, J. Y. and Chaudhury, M. K., *J. R. Soc. Interface* **2**, 55–61 (2005).
- [35] Sarkar, J., Shenoy, V., and Sharma, A., *Phys. Rev. Lett.* **93**, 018302 (2004).
- [36] Sarkar, J., Sharma, A., and Shenoy, V., *Langmuir* **21**, 1457–1469 (2005).
- [37] Sarkar, J., Shenoy, V., and Sharma, A., *Phys. Rev. E* **67**, 031607 (2003).
- [38] Timoshenko, S. P. and Goodier, J. N., *Theory of Elasticity*, 3rd ed. (McGraw-Hill, New York, 1970).
- [39] Dillard, D. A., *J. Appl. Mech.* **56**, 382–386 (1989).
- [40] Ghatak, A., Mahadevan, L., Chung, J. Y., Chaudhury, M. K., and Shenoy, V., *Proc. R. Soc. Lond. A* **460**, 2725–2735 (2004).
- [41] Landau, L. D. and Lifshits, E. M., *Theory of Elasticity*, 3rd ed. (Butterworth-Heinemann, Oxford, 1995).
- [42] Autumn, K., Liang, A. Y., Hsieh, S. T., Zesch, W., Chan, W. P., Kenny, T. W., Fearing, R., and Full, R. J., *Nature* **405**, 681–685 (2000).
- [43] Scherge, M. and Gorb, S., *Proc. R. Soc. Lond. B* **267**, 1239–1244 (2000).
- [44] Federle, W., Brainerd, E. L., McMahon, T. A., and Holldobler, B., *Proc. Natl. Acad. Sci. USA* **98**, 6215–6220 (2001).
- [45] Autumn, K., Sitti, M., Liang, Y. A., Peattie, A. M., Hansen, W. R., Sponberg, S., Kenny, T. W., Fearing, R., Israelachvili, J. N., and Full, R. J., *Proc. Natl. Acad. Sci. USA* **99**, 12252–12256 (2002).
- [46] Sitti, M. and Fearing, R. S., *J. Adhes. Sci. Technol.* **17**, 1055–1073 (2003).
- [47] Peressadko, A. and Gorb, S., *J. Adhes.* **80**, 247–261 (2004).

- [48] Glassmaker, N. J., Jagota, A., Hui, C. Y., and Kim, J., *J. R. Soc. Interface* **1**, 23–33 (2004).
- [49] Gao, H. J. and Yao, H. M., *Proc. Natl Acad. Sci. USA* **101**, 7851–7856 (2004).
- [50] Spolenak, R., Gorb, S., Gao, H. J., and Arzt, E., *Proc. R. Soc. Lond. A* **461**, 305–319 (2005).
- [51] Lake, G. J. and Thomas, A. G., *Proc. R. Soc. Lond. A* **300**, 108–119 (1967).
- [52] Gent, A. N. and Tobias, R. H., *J. Polym. Sci. Polym. Phys. Ed.* **20**, 2051–2058 (1982).
- [53] Carre, A. and Schultz, J., *J. Adhes.* **17**, 135–155 (1984).
- [54] She, H., Malotky, D., and Chaudhury, M. K., *Langmuir* **14**, 3090–3100 (1998).
- [55] Chaudhury, M. K., *J. Phys. Chem. B* **103**, 6562–6566 (1999).
- [56] Ghatak, A., Vorvolakos, K., She, H., Malotky, D. L., and Chaudhury, M. K., *J. Phys. Chem. B* **104**, 4018–4030 (2000).